PET-Based Biodistribution and Radiation Dosimetry of Epidermal Growth Factor Receptor–Selective Tracer ^{11}C-PD153035 in Humans

Ningbo Liu[1], Minghuan Li[2], Xiaoyu Li[3], Xue Meng[2], Guoren Yang[4], Shuqiang Zhao[4], Yi Yang[5], Li Ma[4], Zheng Fu[4], and Jinming Yu[1,2]

[1]Department of Radiation Oncology, Tianjin Medical University Cancer Institute and Hospital, Tianjin, China; [2]Department of Radiation Oncology, Shandong Cancer Hospital and Institute, Jinan, China; [3]Department of Pathophysiology, Nanjing Medical University, Nanjing, China; [4]PET-CT Center, Shandong Cancer Hospital and Institute, Jinan China; and [5]Department of Nuclear Medicine, The Second Affiliated Hospital of Soochow University, Suzhou, China

The present study estimated the biodistribution and radiation-absorbed dose of epidermal growth factor receptor (EGFR) radioligand ^{11}C-PD153035 in whole-body PET examinations of healthy volunteers. **Methods:** Two-dimensional whole-body PET was performed on 9 subjects after injection of ^{11}C-PD153035 at 329.3 ± 77.8 MBq (mean ± SD). A total of 12 frames were acquired for approximately 90 min in 7 segments of the body. Regions of interest were drawn on PET images of source organs. Residence time was calculated as the area under the time–activity curve. Radiation dosimetry was calculated from organ residence time by use of MIRDOSE3 software. **Results:** The renal and hepatobiliary systems played important roles in ^{11}C-PD153035 excretion from the body, accounting for the excretion of approximately 23% and 19% of the injected radioactivity, respectively. Blood-pool activity was only moderate and declined over time. Tracer accumulation in the lungs, bone marrow, and muscles was slight, resulting in low background activity in the chest. The organs with the highest radiation-absorbed doses were the urinary bladder and the gallbladder; the effective doses were 6.08E−02 ± 1.85E−02 and 2.40E−02 ± 8.01E−03 mGy/MBq, respectively. The effective dose equivalent was 7.43E−03 ± 1.10E−03 mSv/MBq, and the dose-limiting organ was the urinary bladder. **Conclusion:** On the basis of the estimated absorbed dose, ^{11}C-PD153035 displayed a favorable radiation dose profile in humans and therefore could be used in multiple PET examinations of the same subject per year. ^{11}C-PD153035 is a promising ligand for the investigation of EGFR in humans, especially in chest tumors such as non–small cell lung cancer.

Key Words: ^{11}C-PD153035; PET; EGFR; molecular imaging; dosimetry

J Nucl Med 2009; 50:303–308
DOI: 10.2967/jnumed.108.056556

Received Aug. 1, 2008; revision accepted Nov. 19, 2008.
For correspondence or reprints contact: Jinming Yu, Department of Radiation Oncology, Shandong Cancer Hospital and Institute, Jiyan Rd. 440, Jinan 250117, Shandong Province, P.R. China.
E-mail: studyhard8@sohu.com
COPYRIGHT © 2009 by the Society of Nuclear Medicine, Inc.

Epidermal growth factor (EGF) receptor (EGFR) and EGFR-targeted therapy have been proven to be useful in the management of malignancies, including non–small cell lung cancer (NSCLC), colon carcinoma, and gastrointestinal stromal tumors (*1,2*). Tyrosine kinase (TK) inhibitors (TKIs), especially derivatives of quinazoline, have been developed as powerful EGFR-targeted drugs; gefitinib and erlotinib are the most extensively evaluated TKIs. These new agents can specifically bind to the intraendothelial TK domain of EGFR and consequently block the signaling pathway (*3*), but the clinical data on TKIs indicate significant variability. There are still no suitable biologic markers or imaging modalities that can be used to objectively monitor or predict treatment responses with this new class of cancer therapy (*4*).

Molecular imaging differs greatly from traditional anatomic imaging. It can visually represent, characterize, and quantify biologic processes at the cellular or subcellular level. Several modalities (PET, SPECT, and MRI) have been introduced to noninvasively investigate EGFR. Among these modalities, PET is the most advanced and practical method for the in vivo measurement of EGFR (*5*). On the basis of EGFR-selective TKIs, a series of PET ligands have been described for EGFR imaging; ^{11}C-labeled-4-*N*-(3-bromoanilino)-6,7-dimethoxyquinazoline (^{11}C-PD153035) has been the most successful (*6*). Johnstrom et al. first radiolabeled PD153035 with isotope ^{11}C at the 6-*O*-methoxy position of the molecule (*7*). ^{11}C-PD153035 demonstrated high affinity and selectivity for EGFR in vitro and in tumor-bearing animal models (*8,9*). Our previous work with tumor-bearing mice and rats confirmed that ^{11}C-PD153035 was rapidly eliminated in the blood pool after intravenous injection and that tracer accumulation in the tumor mass was correlated with EGFR expression (*10*). Moreover, initial data from our clinical study indicated that

^{11}C-PD153035 could be used to noninvasively detect EGFR expression in patients with NSCLC (*11*).

In clinical and basic science studies, EGFR has been detected and quantified by PET with the radioligand ^{11}C-PD153035. The acceptable radiation dose in humans has been estimated by extrapolation of dosimetry data from rodents, but there is no support for this extrapolation. To enable the continued use of ^{11}C-PD153035 and to confirm its safety, we believe that it is important to determine the radiation exposure caused by such studies. Therefore, to further investigate EGFR molecular imaging, we performed the present study to provide a detailed characterization of the biodistribution and radiation dosimetry of ^{11}C-PD153035 in healthy human volunteers.

MATERIALS AND METHODS

Radiopharmaceutical Preparation

The general procedures for the synthesis and ^{11}C radiolabeling of PD153035 (ABX GmbH) were performed with a Tracer Lab FXc system (GE Healthcare) as described previously (*9*). In brief, ^{11}C-carbon dioxide was produced by use of a cyclotron (Minitrace; GE Healthcare) with 9.6-MeV protons. Radiolabeling was successfully performed by alkylation of the phenol group with ^{11}C-methyl iodide under standard methylation conditions. The total synthesis time was approximately 41.2 ± 3.9 (mean ± SD) min (n = 9). The final products were obtained with a radiochemical yield of 36%−51%, a radiochemical purity of 99%, and a chemical purity of 96%. For application in humans, ^{11}C-PD153035 was purified by high-pressure liquid chromatography and diluted in 10 mL of sterile saline.

Subjects

This study was approved by the Institutional Review Board of Shandong Cancer Hospital and Institute and the local radiation protection authorities. Subjects provided written informed consent after receiving an explanation of the study. Nine healthy human volunteers (5 women and 4 men; age, 28.3 ± 3.8 y; age range, 21–32 y) participated in the study from April 2007 to May 2008 (Table 1). All subjects were free of current medical and psychiatric illnesses, as determined from a history, a physical examination, routine laboratory tests (including a complete blood count, blood chemistry, urinalysis, urine drug screening, and hepatitis B tests), and an electrocardiogram. Furthermore, after completion of the PET scan, standard screening laboratory tests were repeated for every subject.

TABLE 1. Subject Characteristics

Subject or parameter	Age (y)	Height (cm)	Weight (kg)	Injected dose (MBq)	Sex
1	31	168	62	314.5	F
2	21	178	73	292.3	M
3	29	174	82	447.7	M
4	32	176	72	436.6	M
5	31	158	61	240.5	F
6	28	165	64	303.4	F
7	27	169	63	281.2	F
8	31	174	75	251.6	M
9	25	163	69	395.9	F
Mean ± SD	28.3 ± 3.8	169.4 ± 6.6	65.4 ± 7.7	329.3 ± 77.8	

PET Procedure

PET scans were performed with a PET/CT scanner (Discovery LS; GE Healthcare) capable of multislice helical CT. Coregistered CT and PET images were acquired in one session, and patients were examined in the supine position. A low-dose CT scan was performed before tracer administration to correct for photon attenuation and to provide an anatomic reference (*12*). After injection of ^{11}C-PD153035 at 329.3 ± 77.8 MBq, a series of 12 whole-body scans were obtained. Each scan consisted of 7 bed positions (15-cm field of view) and covered the area from the head to the midthigh of the body. In each bed position, data were acquired for 1 min in the 2-dimensional mode. The total acquisition time was approximately 90 min. Positron emission data were reconstructed on a 128 × 128 matrix (slice thickness, 4.25 mm) by use of the ordered-subsets expectation maximization algorithm with 8 iterations and 4 subsets. The standardized uptake value (SUV) was calculated with the following formula: [measured activity concentration (Bq/mL) × body weight (kg)]/injected activity (Bq). Calculation of the radioactivity concentration included the use of a calibration factor that converted the activity counts into becquerels, and the decay correction of the commercial reconstruction software (Xeleris workstation; GE Healthcare) was removed. Electrocardiography findings, heart rates, blood pressure, and respiration rates were monitored for all subjects during scanning.

Residence Time Calculation

Organs included in the analysis were those determined by visual inspection as having activity exceeding that of the background. Images were calibrated to Bq/mL with the following steps: draw regions of interest (ROIs) manually on each slice of a given organ on PET images (use CT images as an anatomic reference), sum the radioactivities in all ROIs for each organ, calculate the volumes of the organs by use of PMOD software (PMOD Technologies Ltd.), and divide the sum of the radioactivities by the volume of each organ (*13*). The same ROIs were copied to the serially acquired images of each organ to form the time–activity curve (Bq/mL vs. time). The area under the curve for each organ from zero to infinity was equal to the residence time (in h). All activity in the heart ROI was conservatively assumed to be in the heart wall. The small intestine was sampled in the duodenum, which had the highest activity in the small intestine. All activity that was not accounted for was assumed to be indefinitely retained in the remainder of the body. Organ activity curves were fitted to either mono- or biexponential functions.

Organ Absorbed Dose Estimate

Urination was not allowed during scanning; therefore, the activity overlying the bladder represented total urinary excretion. The MIRD algorithm was implemented in the MIRDOSE3 program (Oak Ridge Institute for Science and Education) by using the residence time calculated as described earlier (*14,15*). The organ absorbed dose estimate was based on the 70-kg reference adult phantom developed by Cristy and Eckerman (*16*). The S value was determined by use of the standard MIRD approach. The effective dose equivalent and the effective dose were calculated for each subject.

RESULTS

Injection of ^{11}C-PD153035 caused no significant changes in heart rates, respiration rates, and blood pressure. Figure 1 shows a representation of a coronal section from whole-body PET and the distribution of ^{11}C-PD153035 in a healthy volunteer. The biodistribution and accumulation of ^{11}C-PD153035 in a patient with NSCLC are shown in Figure 2. Figure 3 shows a representative set of tissue time–activity curves (SUV vs. time). The highest SUVs in solid organs 60 min after injection were found in the bladder (SUV, 5.29 ± 1.09), followed by the gallbladder (SUV, 2.67 ± 1.06), the kidneys (SUV, 2.15 ± 0.69), the bile secreted into the small intestine (SUV, 1.88 ± 0.78), and the liver (SUV, 1.09 ± 0.81). Low activities were found in the lungs and muscles 60 min after injection, with SUVs of 0.22 ± 0.07 and 0.14 ± 0.05, respectively. In the liver and kidneys, there was some retention of activities over time. In contrast, in the spleen, a rapid decrease in activity over time was found, paralleling the decrease in blood-pool activity. We found the renal system and the hepatobiliary system to be important in the clearance of ^{11}C-PD153035 from the body, accounting for the excretion of approximately 23% and 19% of the injected radioactivity, respectively. Of the excreted ^{11}C activity at 60 min, approximately 60% was eliminated through the urinary tract and 40% was eliminated through the hepatobiliary system. In general, the area of highest activity was the urogenital tract (kidneys, ureters, and bladder), followed by the liver, gallbladder, and small intestine. Blood-pool activity was only moderate and declined over time. Background activities in the muscles and lungs were low.

In the liver and kidneys, the clearance of radioactivity after the initial increase was adequately fitted to a decaying monoexponential curve. In the gallbladder, small intestine, urinary bladder, and ureters, the time courses were more protracted and were fitted to biexponential curves. The average residence times for the urinary bladder, liver, small intestine, kidneys, gallbladder, red marrow, heart wall, brain, and lungs were 9.02E−02 ± 2.75E−02, 5.19E−02 ± 9.87E−03, 1.64E−02 ± 4.39E−03, 1.51E−02 ± 7.24E−03, 9.63E−03 ± 3.44E−03, 1.89E−03 ± 7.03E−04, 1.85E−03 ± 7.27E−04, 1.56E−03 ± 6.58E−04, and 2.48E−04 ± 1.56E−04 h, respectively.

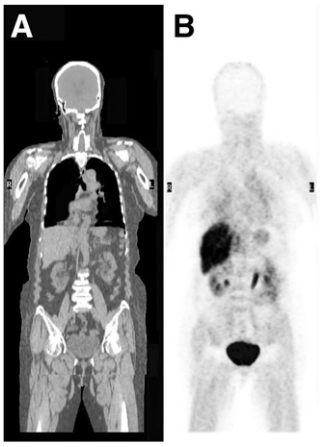

FIGURE 1. Representative coronal images of whole-body biodistribution of ^{11}C-PD153035 30–40 min after injection (292.3 MBq) in healthy volunteer. Intense tracer uptake was observed in liver, gallbladder, urinary bladder, and kidneys. (A) CT image. (B) PET image.

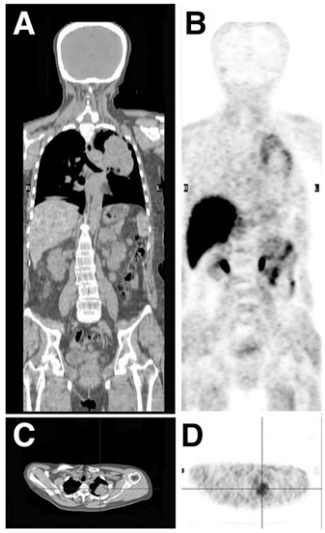

FIGURE 2. ^{11}C-PD-153035 PET/CT scan in patient with NSCLC of left lung. (A) Coronal CT image. (B) Coronal PET image. (C) Transaxial CT image. (D) Transaxial PET image.

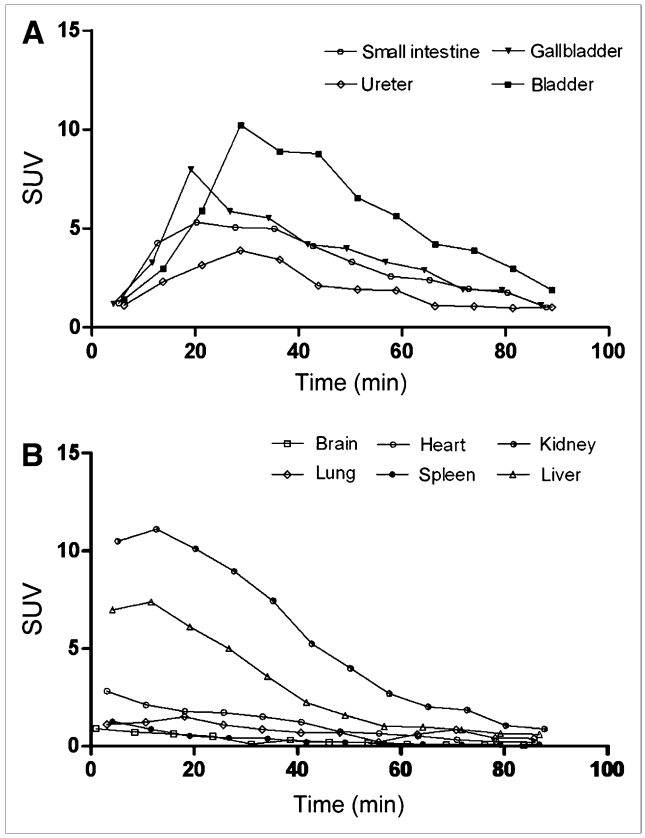

FIGURE 3. (A) Time–activity curves for ^{11}C-PD153035 in serial PET of gallbladder, bladder, small intestine, and ureter. Data points indicate measured mean activities and were not corrected for radioactive decay. (B) Time–activity curves for ^{11}C-PD153035 in serial PET of liver, kidneys, brain, lungs, heart, and spleen. Data points indicate measured mean activities and were not corrected for radioactive decay.

Table 2 shows the average radiation-absorbed doses calculated for all organs from the individual organ residence times. The highest absorbed dose was found in the urinary bladder wall (6.08E−02 ± 1.85E−02 mGy/MBq), followed by the gallbladder wall (2.40E−02 ± 8.01E−03 mGy/MBq), kidneys (1.42E−02 ± 6.36E−03 mGy/MBq), and liver (9.10E−03 ± 1.65E−03 mGy/MBq). This finding confirmed that the tracer was predominantly excreted through the renal pathway. The effective dose equivalent was 7.43E−03 ± 1.10E−03 mSv/MBq, and the dose-limiting organ (the organ with the highest absorbed dose) was the urinary bladder.

DISCUSSION

^{11}C-PD153035 was first described in 1998 (*7*) and was further verified as an EGFR imaging agent in many studies (*8–11,17,18*). Our previous studies showed that the uptake of ^{11}C-PD153035 in vitro or in vivo was closely correlated with the EGFR expression level and that the images could be analyzed by the ROI technique (*9,10*). Recently, our pilot studies of patients with NSCLC showed that there was a significant difference in ^{11}C-PD153035 uptake between the tumor mass and healthy tissue. Immunohistochemical analysis confirmed EGFR expression in tumors with ^{11}C-PD153035 uptake, and the SUVs were also correlated with the EGFR expression level (*11*).

The results of the present study demonstrated promising distribution and radiation dosimetry of ^{11}C-PD153035 in healthy human volunteers. The data showed that the high uptake of ^{11}C-PD153035 initially occurring in the renal and hepatobiliary systems contributed to the relatively high radiation burden in these organs. The distribution of radioactivity in peripheral organs did not match the EGFR expression level. It is possible that most of the activity detected in peripheral organs in the present study was from radioactive metabolites not binding to the receptor. Our data demonstrated that the main route of elimination of the tracer was the urinary tract, followed by the hepatobiliary pathway, a pattern of excretion similar to that in the mouse model. This finding was not surprising, given the lipophilicity of PD153035. Low uptake in the lungs and rapid clearance from the blood pool resulted in high-quality images and reliable statistics for quantification in the chest. Thus, ^{11}C-PD153035 may be an excellent radiotracer for lung cancer, especially NSCLC. However, tracer accumulation in the liver, gallbladder, kidneys, urinary bladder, and ureters led to low contrast in the abdomen. This wide distribution of ^{11}C-PD153035 in the abdominal region of humans obviates its usefulness for the imaging of abdominal tumors. Tumor metastasis in the liver or lymph nodes cannot be displayed well by ^{11}C-PD153035 PET.

Moreover, there are still some incompatibilities between ^{11}C-PD153035 distribution in humans and that in rodent models (*9,10*). Tracer accumulation in the human lungs and brain was lower than that in mice and rats. The underlying mechanisms of this difference in distributions remain unclear. Species differences and differences in the pathway of ^{11}C-PD153035 metabolism may contribute to this discrepancy. For example, rats do not have a gallbladder, so that a rat study either has no tracer distribution for that organ or requires an approximation based on a biliary excretion model and a measurement from the small intestine. Samén (*6*) et al. incubated samples containing the 6- and 7-*O*-methoxy positions of ^{11}C-PD153035 with rodent and human liver microsomes in vitro. The differences observed in their incubations suggested that in vivo ^{11}C-PD153035 PET studies in rodents may not be directly predictive for studies in humans. The differences in the pathway of ^{11}C-PD153035 metabolism strongly suggest that more work should be focused on this area.

TABLE 2. Mean Radiation-Absorbed Dose Estimates for ^{11}C-PD153035

Organ or parameter	Mean ± SD radiation-absorbed dose (mGy/MBq)		
	Men	Women	Average
Adrenal glands	1.10E−03 ± 9.49E−05	1.05E−03 ± 1.42E−04	1.07E−03 ± 1.19E−04
Brain	3.92E−04 ± 1.07E−04	3.43E−04 ± 1.88E−04	3.65E−04 ± 1.50E−04
Gallbladder wall	2.69E−02 ± 1.10E−02	2.16E−02 ± 4.74E−03	2.40E−02 ± 8.01E−03
Small intestine	5.38E−03 ± 9.00E−05	6.00E−03 ± 1.82E−03	5.73E−03 ± 1.33E−03
Heart wall	1.79E−03 ± 3.62E−04	2.03E−03 ± 8.05E−04	1.93E−03 ± 6.24E−04
Kidneys	1.62E−02 ± 7.02E−03	1.25E−02 ± 6.06E−03	1.42E−02 ± 6.36E−03
Liver	8.93E−03 ± 1.71E−03	9.24E−03 ± 1.78E−03	9.10E−03 ± 1.65E−03
Lungs	4.10E−04 ± 3.62E−05	4.41E−04 ± 9.00E−05	4.27E−04 ± 6.93E−05
Muscles	5.21E−04 ± 1.09E−04	6.35E−04 ± 8.93E−05	5.84E−04 ± 1.10E−04
Pancreas	1.45E−03 ± 2.33E−04	1.52E−03 ± 2.99E−04	1.49E−03 ± 2.58E−04
Red marrow	7.29E−04 ± 6.42E−05	7.53E−04 ± 1.19E−04	7.42E−04 ± 9.37E−05
Spleen	2.32E−03 ± 2.85E−04	2.72E−03 ± 1.31E−03	2.54E−03 ± 9.68E−04
Urinary bladder wall	4.93E−02 ± 1.90E−02	7.00E−02 ± 1.32E−02	6.08E−02 ± 1.85E−02
Ovaries		1.87E−03 ± 3.25E−04	1.87E−03 ± 3.25E−04
Testes	7.23E−04 ± 2.67E−04		7.23E−04 ± 2.67E−04
Effective dose equivalent (mSv/MBq)	6.94E−03 ± 1.38E−03	7.82E−03 ± 7.33E−04	7.43E−03 ± 1.10E−03
Effective dose (mSv/MBq)	3.98E−03 ± 1.21E−03	5.24E−03 ± 8.40E−04	4.68E−03 ± 1.16E−03

As a consequence of the biodistribution, the urinary bladder and the gallbladder were the organs with the highest absorbed doses. The amount of ^{11}C-PD153035 injected, about 330 MBq, resulted in an effective dose equivalent of about 7 mSv/MBq. This low value would allow multiple serial examinations of the same subject. According to the intramural guidelines of the National Institutes of Health, adult research subjects should receive no more than a 50-mSv (5-rem) effective dose per year (*19*). With regard to our results, this 50-mSv limit would allow as many as 7 EGFR scans of a subject in a single year. These findings suggest the possibility of very efficient interventional studies, such as evaluation of the therapeutic effect of EGFR-targeted therapy or receptor occupancy studies with new drugs aimed at interfering with EGFR.

Concerning radiation protection, ^{11}C-PD153035 also compared favorably with other radiotracers (*12,13*). Furthermore, the absence of effects on vital signs (heart rate and blood pressure) after intravenous injection indicated that ^{11}C-PD153035 is also safe from a pharmacologic perspective.

The radiation dose results obtained in the present study with the MIRDOSE3 program were for a reference 70-kg adult man. The organ sizes of our subjects may have been smaller than those of a reference 70-kg adult man. Therefore, the observed organ radioactivity concentrations and relative distributions in the body likely were somewhat overestimated. The assumption for the small intestine was made by equating the mean activity with the activity observed in the duodenum, which had a relatively high tracer accumulation; therefore, the residence time in the small intestine likely was also somewhat overestimated. A possible error in our radiation dose calculation might result from curve fitting, especially for organs with low retention of the tracer, because of our scanning method. An early perfusion phase might be missed by our 1-min scan time per bed position and might cause increases in the residence time and the effective dose equivalent (*12*). Although such an error is a concern, the effective dose equivalent for ^{11}C-PD153035 is safe for research or medical purposes.

EGFR antibody and EGF can be radiolabeled as EGFR molecular imaging probes (*20–23*). However, they can only detect the level of EGFR expression on the cell membrane; they cannot detect intracellular TK activity directly or determine the status of the EGFR signaling pathway accurately. Other quinazoline derivatives, including ^{18}F-gefitinib, were previously demonstrated to be candidates for EGFR imaging as well (*24–26*). However, rapid metabolism and nonspecific binding to the target receptor kinase made most of these agents ineffective as tracers for EGFR imaging, although some in vitro experiments indicated efficacy. Wang et al. (*27*) and Holt et al. (*28*) independently developed ^{11}C-gefitinib and provided a foundation for the further evaluation of ^{11}C-gefitinib as a potential PET probe. In vitro and in vivo studies of ^{11}C-gefitinib are currently under way. None of the TKI tracers except for ^{11}C-PD153035 has been reported in a clinical trial of EGFR imaging. To our limited knowledge, ^{11}C-PD153035 might have the most potential for the imaging of EGFR, especially the TK activity of its signaling pathway.

CONCLUSION

^{11}C-PD153035 is rapidly cleared from the body, largely by the kidneys and liver. The effective radiation dose is substantially lower than the estimated maximum radiation burden caused by ^{11}C tracers. This finding means that serial examinations of the same subject seem feasible from the viewpoint of radiation safety. ^{11}C-PD153035 is a promising ligand for the investigation of EGFR in humans, especially in chest tumors such as NSCLC.

ACKNOWLEDGMENTS

We thank the staff of the PET-CT Center, Shandong Cancer Hospital and Institute, particularly Anqin Han and Jinsong Zheng, for their technical support. This work was supported by The National High Technology Research and Development Program of China (grant 2007AA02Z437).

REFERENCES

1. Normanno N, De Luca A, Bianco C, et al. Epidermal growth factor receptor (EGFR) signaling in cancer. *Gene.* 2006;366:2–16.
2. Ettinger DS. Clinical implications of EGFR expression in the development and progression of solid tumors: focus on non-small cell lung cancer. *Oncologist.* 2006;11:358–373.
3. Fry DW, Kraker AJ, McMichael A, et al. A specific inhibitor of the epidermal growth factor receptor tyrosine kinase. *Science.* 1994;265:1093–1095.
4. Marchetti A, Martella C, Felicioni L, et al. EGFR mutations in non-small-cell lung cancer: analysis of a large series of cases and development of a rapid and sensitive method for diagnostic screening with potential implications on pharmacologic treatment. *J Clin Oncol.* 2005;23:857–865.
5. Hoffman JM, Gambhir SS. Molecular imaging: the vision and opportunity for radiology in the future. *Radiology.* 2007;244:39–47.
6. Samén E, Thorell JO, Fredriksson A, Stone-Elander S. The tyrosine kinase inhibitor PD153035: implication of labeling position on radiometabolites formed in vitro. *Nucl Med Biol.* 2006;33:1005–1011.
7. Johnstrom P, Fredriksson A, Thorell JO, et al. Synthesis of [methoxy-^{11}C]PD153035, a selective EGF receptor tyrosine kinase inhibitor. *J Labelled Comp Radiopharm.* 1998;41:623–629.
8. Fredriksson A, Johnstrom P, Thorell JO, et al. In vivo evaluation of the biodistribution of ^{11}C-labeled PD153035 in rats without and with neuroblastoma implants. *Life Sci.* 1999;65:165–174.
9. Wang H, Yu JM, Yang GR, et al. Assessment of ^{11}C-labeled-4-*N*-(3-bromoanilino)-6,7-dimethoxyquinazoline as a positron emission tomography agent to monitor epidermal growth factor receptor expression. *Cancer Sci.* 2007;9:1413–1416.
10. Wang H, Yu JM, Yang GR, et al. Further characterization of the epidermal growth factor receptor ligand ^{11}C-PD153035. *Chin Med J (Engl).* 2007;120:960–964.
11. Yu JM, Liu NB, Yang GR, et al. ^{11}C-PD153035 PET/CT for molecular imaging of EGFR in patients with non-small cell lung cancer (NSCLC) [abstract]. *J Clin Oncol.* 2008;26(suppl):15S.
12. Treyer V, Streffer J, Ametamey SM, et al. Radiation dosimetry and biodistribution of ^{11}C-ABP688 measured in healthy volunteers. *Eur J Nucl Med Mol Imaging.* 2008;35:766–770.
13. Cropley VL, Fujita M, Musachio JL, et al. Whole-body biodistribution and estimation of radiation-absorbed doses of the dopamine D_1 receptor radioligand ^{11}C-NNC112 in humans. *J Nucl Med.* 2006;47:100–104.
14. Stabin MG. MIRDOSE: personal computer software for internal dose assessment in nuclear medicine. *J Nucl Med.* 1996;37:538–546.

15. Beer AJ, Haubner R, Wolf I, et al. PET-based human dosimetry of ^{18}F-galacto-RGD, a new radiotracer for imaging αvβ3 expression. *J Nucl Med.* 2006;47: 763–769.
16. Cristy M, Eckerman KF. *Specific Absorbed Fractions of Energy at Various Ages from Internal Photon Sources.* Oak Ridge, TN: Oak Ridge National Laboratory; 1987.
17. Mishani E, Abourbeh G. Cancer molecular imaging: radionuclide-based biomarkers of the epidermal growth factor receptor (EGFR). *Curr Top Med Chem.* 2007;7:1755–1772.
18. Mulholland G, Zheng Q, Winkle WL, et al. Synthesis and biodistribution of new C-11- and F-18-labeled epidermal growth factor receptor ligands [abstract]. *J Nucl Med.* 1997;38(suppl 5):141P.
19. International Commission on Radiological Protection. *Radiological Protection and Safety in Medicine.* Oxford, U.K.: Pergamon Press; 1996. ICRP Publication 73.
20. Vallis KA, Reilly RM, Chen P, et al. A phase I study of ^{99m}Tc-hR3 (DiaCIM), a humanized immunoconjugate directed towards the epidermal growth factor receptor. *Nucl Med Commun.* 2002;23:1155–1164.
21. Dadparvar S, Krishna L, Miyamoto C, et al. Indium-111-labeled anti-EGFr-425 scintigraphy in the detection of malignant gliomas. *Cancer.* 1994;73(suppl 3): 884–889.
22. Cai W, Chen K, He L, et al. Quantitative PET of EGFR expression in xenograft-bearing mice using ^{64}Cu-labeled cetuximab, a chimeric anti-EGFR monoclonal antibody. *Eur J Nucl Med Mol Imaging.* 2007;34:850–858.
23. Niu G, Cai W, Chen K, et al. Non-invasive PET imaging of EGFR degradation induced by a heat shock protein 90 inhibitor. *Mol Imaging Biol.* 2008;10:99–106.
24. Mishani E, Abourbeh G, Jacobson O, et al. High-affinity epidermal growth factor receptor (EGFR) irreversible inhibitors with diminished chemical reactivities as positron emission tomography (PET)-imaging agent candidates of EGFR overexpressing tumors. *J Med Chem.* 2005;48:5337–5348.
25. Bonasera TA, Ortu G, Rozen Y, et al. Potential ^{18}F-labeled biomarkers for epidermal growth factor receptor tyrosine kinase. *Nucl Med Biol.* 2001;28:359–374.
26. Su H, Seimbille Y, Ferl GZ, et al. Evaluation of [^{18}F]gefitinib as a molecular imaging probe for the assessment of the epidermal growth factor receptor status in malignant tumors. *Eur J Nucl Med Mol Imaging.* 2008;35:1089–1099.
27. Wang JQ, Gao M, Kathy D, et al. Synthesis of ^{11}C-Iressa as a new PET cancer imaging agent for epidermal growth factor receptor tyrosine kinase. *Bioorg Med Chem Lett.* 2006;16:4102–4106.
28. Holt DP, Ravert HT, Dannals RF, et al. Synthesis of [^{11}C]gefitinib for imaging epidermal growth factor receptor tyrosine kinase with positron emission tomography. *J Labelled Comp Radiopharm.* 2006;49:883–888.